

Full length article

Analysis of bi-directional functionally graded plates by FEM and a new third-order shear deformation plate theory



Thom Van Do^a, Dinh Kien Nguyen^b, Nguyen Dinh Duc^{c,d}, Duc Hong Doan^{c,*}, Tinh Quoc Bui^{e,f,**}

^a Department of Mechanics, Le Quy Don Technical University, 236 Hoang Quoc Viet, Hanoi, Vietnam

^b Institute of Mechanics, VAST, 18 Hoang Quoc Viet, Hanoi, Vietnam

^c Advanced Materials and Structures Laboratory, University of Engineering and Technology, Vietnam National University, 144 Xuan Thuy, Cau Giay, Hanoi, Vietnam

^d Infrastructure Engineering Program, VNU Vietnam-Japan University, My Dinh 1, Tu Liem, Hanoi, Vietnam

^e Institute for Research and Development, Duy Tan University, Da Nang City, Vietnam

^f Department of Civil and Environmental Engineering, Tokyo Institute of Technology, 2-12-1-W8-22, Ookayama, Meguro-ku, Tokyo 152-8552, Japan

ARTICLE INFO

Keywords:

2D-FGM

FEA

Buckling

Third-order shear deformation theory

Plates

ABSTRACT

Modern structures and components may require advanced materials whose properties vary continuously not only in one specified direction, but also different other directions. In particular, the bi-directional functionally graded materials (2D-FGMs) introduced are expected to have more effective properties, consequently eliminating commonly awkward problems such as local stress concentrations and delamination. In this paper, buckling and bending behaviors of 2D-FGM plates, which are of great importance in the design and development of engineering applications, are numerically analyzed by a finite element model. The plate kinematics are described using a new third-order shear deformation plate theory (TSDT), without the need for special treatment of shear-locking effect and shear correction factors. The present TSDT theory based on rigorous kinematic of displacements, which is shown to be dominated over other preceding theories, is derived from an elasticity formulation, rather by the hypothesis of displacements. The materials are assumed to be graded in two directions and their effective properties are computed through the rule of mixture. The accuracy of the proposed approach assessed on numerical results is confirmed by comparing the obtained results with respect to reference published solutions. The effects of some numerical aspect ratios such as volume fraction, boundary conditions, thickness to length ratio, etc. on static deflections and critical buckling are numerically studied. The investigation of results confirms that such aforementioned aspect ratios have significant effects on the mechanical behaviors of plates.

1. Introduction

Functionally graded materials (FGMs) or advanced composite materials with graded microstructures whose compositional gradients are fabricated to gain unique characteristics that do not exist in their constituent materials, are widely used in many engineering applications. Some major advantages of the FGMs are, for instance, the elimination of delamination mode of failure, residual stresses, high inter-laminar shear stresses, local stress concentration at interface, or reducing thermal stress, which persists in laminated composites [1,2].

The plates are widely used in different structures, and are very important structural elements used in many engineering applications such as civil, aerospace, marine structures, and automobile. Consequently, it thus is crucial to study mechanical behaviors of functionally graded plates under mechanical loading condition, which

is to optimize their resistance to damage. In the last few decades, scientists and researchers have paid much attention to the investigation of the structural responses of plates using experimental, numerical and theoretical approaches. In fact, the studies of linear and nonlinear mechanical behaviors of FGMs structures under static or dynamic loading conditions are fairly well presented in literature, e.g., see [1–11,37–40], just to name a few. Different plate theories including the first-order shear deformation theory (FSDT) or higher-order theories have been introduced and used to describe plate kinematics. In those cited papers, the material properties are assumed to continuously vary in only one specified direction.

However, modern structures and components may require advanced materials whose properties vary continuously not only in one specified direction, but also different other directions. In that sense, the bi-directional functionally graded materials (2D-FGMs) are introduced in

* Corresponding author at: University of Engineering and Technology, VNU, Vietnam.

** Corresponding author at: Duy Tan University, Vietnam & Tokyo Institute of Technology, Japan.

E-mail addresses: doan.d.aa.eng@gmail.com (D.H. Doan), buiquoctinh@duytan.edu.vn, bui.t.aa@m.titech.ac.jp (T.Q. Bui).

the literature, e.g., see [12–15], which are expected to have more effective properties, consequently eliminating commonly awkward problems, for instance, local stress concentrations or delamination. As stated by Nemat-Alla in [12], the conventional one-dimension FGMs may not be so effective in the design of advanced applications in propulsion systems and in airframes for space applications, which often operate in high temperature variations in two or three directions. The underlying idea of adding a third material constituent to the conventional FGMs as introduced in [12] is to withstand the induced severe thermal stresses. Such 2D-FGMs bring superior characteristics as it has been shown in their numerical experiments that 2D-FGMs have higher capability to reduce thermal stresses than the conventional ones. One important point must be noticed that all works reported in [13–15] have considered exponential functions for continuous gradation of the material properties, which usually facilitate analytical solutions but do not represent real properties of materials, except at the lower and upper surfaces of 2D-FGMs. The rules of mixture and volume fractions relations introduced in [12], however offer a means that much better represents the material properties of 2D-FGMs.

Recently, many studies and investigations related to 2D-FGMs have been carried out and available in literature. For instance, Nemat-All [16] extended his work to study the reduction of thermal stresses by composition optimization for $ZrO_2/6061-T6/Ti-6Al-4V$ 2D-FGMs under a severe thermal loading cycle using a finite element model. In the same year, 2009, he and his co-workers [17] used their finite element model to numerically analyze the elasto-plastic behaviors of 2D-FGMs under thermal loading. Asgari and Akhlaghi [18] investigated natural frequencies of 2D-FGM thick hollow cylinder based on three-dimensional elasticity equations, while analytical methods, the generalized differential quadrature (GDQ) and generalized integral quadrature (GIQ), are applied to study natural frequency of 2D-FGMs cylindrical shells by Ebrahimi and Najafzadeh [19]. Dynamic responses of 2D-FGMs thick hollow cylinder with finite length under impact loading are analyzed using graded finite elements [20]. Lü et al. [21] presented a semi-analytical investigation for orthotropic multi-directional FGMs plates using the differential quadrature method (DQM). Shariyat and Jafari [22] proposed a refined contact stiffness approach to study nonlinear low-velocity impact response of a radially preloaded 2D-FGM circular plate. Qian and Batra [23] used a higher-order shear and normal deformable plate theory and a meshless local Petrov-Galerkin method to find the compositional profile of 2D-FGM plates, which is for optimal natural frequencies. More recently, a theoretical analysis of buckling behavior of 2D-FGM cylindrical shells reinforced by axial stiffeners using a TSDT is reported in [24], while the meshfree radial point interpolation method (RPIM) to extract three-dimensional frequency of 2D-FGM thick cylindrical shells is presented in [25]. In addition, the concept of 2D-FGMs is also recently applied to Timoshenko beams [26–28], or Euler-Bernoulli nano-beams [29,30]. The NURBS isogeometric finite element approach, a recent effective numerical method, is alternatively used for analysis of fully coupled thermo-mechanical behavior of 2D-FGMs beams [31]. More interestingly, the conventional 1D-FGMs and 2D-FGMs is also found to have been applied to biomedical engineering problems, for backing shells of cemented acetabular cup, reported by Hedia [32]. Nevertheless, it is easily realized that numerical studies of static bending and buckling behaviors of 2D-FGM plates using finite element methods are rather rare in literature, and it thus is the main subject being reported in this manuscript. As it is well known that when a plate subjected to in-plane compression or shear loads, it may lose its stability once the loads reach a critical value [33]. This phenomenon is known as buckling, and detailed assessments of its behaviors for 2D-FGM plates are of importance to the design and development of engineering applications.

The present manuscript is devoted to the development of an accurate numerical approach using FEM and a novel high-order plate theory for static bending and buckling behaviors of 2D-FGM plates under statically mechanical loading. In particular, the plate kinematics

presented are described using a new effective third-order shear deformation plate theory (TSDT) recently introduced by Shi [34], without the need for special treatment of shear-locking effect and shear correction factors. The adopted TSDT theory based on rigorous kinematic of displacements, which is shown to be dominated over other preceding theories, is derived from an elasticity formulation, rather by the hypothesis of displacements. The materials are assumed to be graded in two directions and the effective properties are computed using the rule of mixture. In the numerical applications, we will analyze the static bending deflections, critical buckling coefficients, and explore the effects of various numerical aspect ratios such as gradient volume fraction, thickness-to-length ratio, boundary conditions, etc. on the mechanical behaviors of 2D-FGM plates. We will further visualize and investigate the distribution of stresses across the plates, which is to additionally extract insight into the physical phenomena of bending plates. In addition, the buckling modes of 2D-FGM plates are depicted as well.

One must be noticed that there are many different plate theories, from classical to higher order, available in literature, but preceding studies have proved that the third-order shear deformation theories (TSDTs) are one of the effective and accurate methods [10]. It is because the TSDTs deal with a quadratic vibration of transverse shear strains and stresses across the thickness, and they do not require a shear correction factor. The new TSDT recently presented by Shi in [34] owns several desirable advantages, especially offering higher accurate solutions than many other higher-order shear deformation plate theories. The Shi's theory is very young and its applications are rather rare. Wattanasakulpong et al. [35,36] presented analytical solutions of thermal buckling, free and forced vibration for both FGM beams and plates by adopting the Shi's theory. Recently, the authors employed the Shi's theory to numerically address high temperature mechanical behaviors of conventional heated FGM plates based on FEM [10].

Following the above introduction, the rest of this paper is as follows. In Section 2, a 2D-FGM plate with the variation of effective properties in thickness and longitudinal direction used in the analysis is described. Section 3 develops a finite element formulation for static and buckling analyses of the 2D-FGM plate. Numerical results on the bending, buckling loads and buckling mode shapes are presented in Section 4. The main conclusions which can be drawn from the paper are summarized in Section 5.

2. Bi-directional functionally graded plates

A rectangular FGM plate with thickness h , length a and width b in a Cartesian co-ordinates (x,y,z) as depicted in Fig. 1 is considered. The xy plane is chosen in the mid-surface of the plate, while the z -axis is directed upwards from the mid-plane. The plate is assumed to be formed from three distinct constituents whose volume fractions, V_1 , V_2 and V_3 , are continuously varied in the thickness and longitudinal direction according to [17]

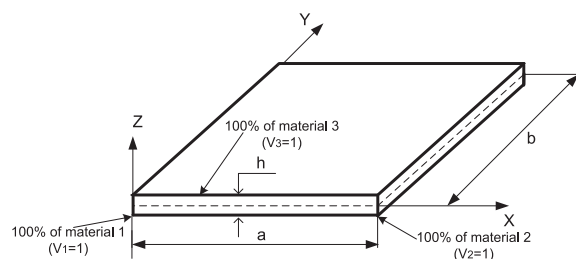


Fig. 1. Geometrical notation of a rectangular 2D-FGM plate.

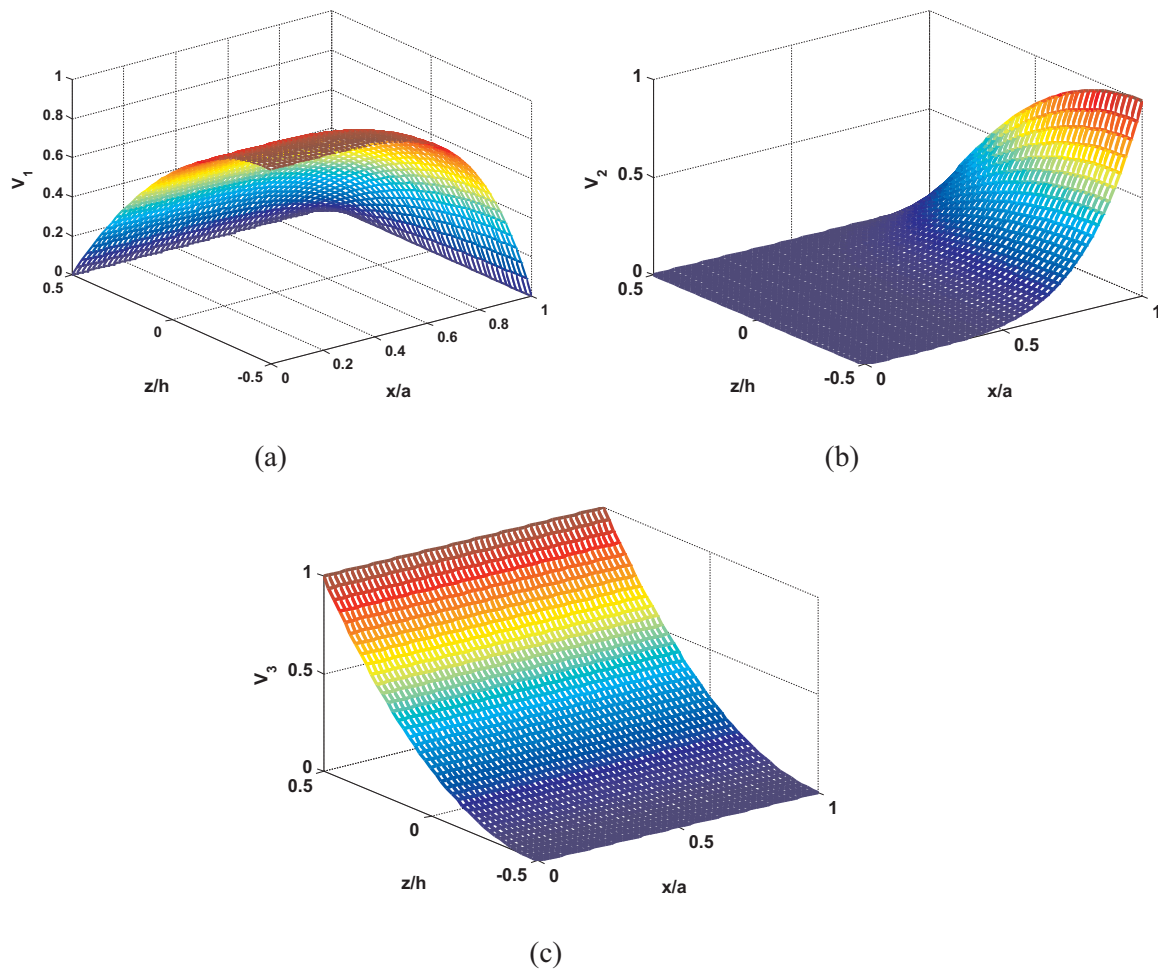


Fig. 2. The distribution of V_1, V_2, V_3 of the 2D FGM plate for $n = 2, q = 5$.

Table 1

Comparison of normalized deflections and normal stress of a fully simply supported Al/Al_2O_3 plate ($a/b = 1, a/h = 10$) for different values of the volume fraction exponent n among different theories: the present, the Reddy's theory [3], the SSDPT [4], and the HSDT [10].

n	\bar{w}				$\bar{\sigma}_{xx}$			
	Reddy [3]	SSDPT[4]	HSDT [10]	This work	Reddy [3]	SSDPT [4]	HSDT [10]	This work
Ceramic	0.4665	0.4665	0.4630	0.4659	2.8920	2.8932	2.8930	2.8930
1	0.9421	0.9287	0.9130	0.9224	4.2589	4.4745	4.3560	4.4441
2	1.2227	1.1940	1.2069	1.1787	4.8889	5.2229	5.0449	5.1795
3	1.3530	1.3200	1.3596	1.2970	5.2055	5.6108	5.2026	5.5462
5	1.4646	1.4356	1.4874	1.4055	5.7066	6.1504	5.8751	6.0696
10	1.6054	1.5876	1.6308	1.5651	6.9540	7.3689	7.1148	7.2863
Metal	2.5328	2.5327	2.5120	2.4968	2.8920	2.8932	2.8930	2.8680

Table 2

Material properties of constituent materials for the 2D-FGM plate.

Material properties	Material 1	Material 2	Material 3
E (GPa)	205.1	70	151
ν	0.3	0.3	0.3

$$V_1 = \left[1 - \left(\frac{z}{h} + \frac{1}{2} \right)^n \right] \left[1 - \left(\frac{x}{a} \right)^q \right], \quad V_2 = \left[1 - \left(\frac{z}{h} + \frac{1}{2} \right)^n \right] \left(\frac{x}{a} \right)^q, \quad V_3 = \left(\frac{z}{h} + \frac{1}{2} \right)^n \quad (1)$$

where q and n are the non-negative gradient indexes that represent the composition variations in x and z directions, respectively.

The composition of the 2D-FGM in Eq. (1) changes through the thickness direction from 100% material 3 at the upper surface, $z = h/2$, to an FGM of two different materials, namely material 1 and material 2, at the bottom surface, $z = -h/2$. The composition of FGM at the bottom surface also changes from 100% material 1 at the left edge, $x = 0$ and $z = -h/2$, to 100% metal 2 at the right edge, $x = a$ and $z = -h/2$. It can be verified from Eq. (1) that when $q = 0$, the present 2D-FGM deduces to the conventional FGM formed from two materials, which has been widely considered in the literature. Particularly, Eq. (1) leads to an axially FGM made of material 2 and material 3 if $q = 0$.

Additionally, the distributions of V_1, V_2, V_3 through the 2D FGM plate when $n = 2, q = 5$ are also depicted in Fig. 2.

Various rules of mixture can be used for evaluating the effective properties of an FGM, and the Voigt's model is adopted in this study.

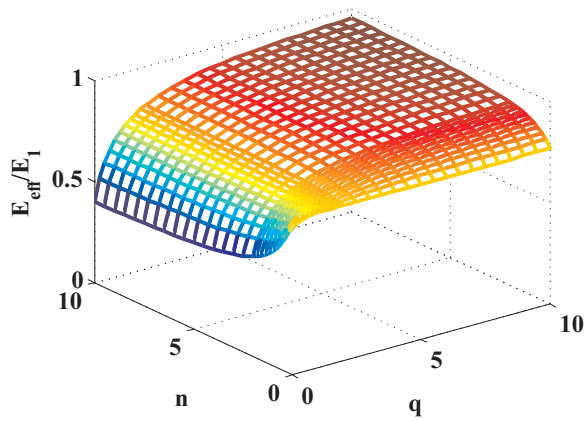
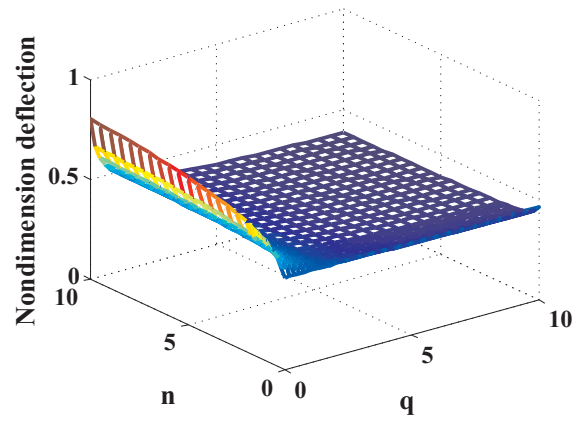
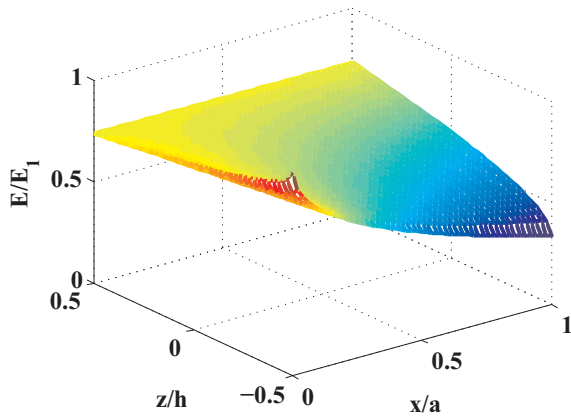


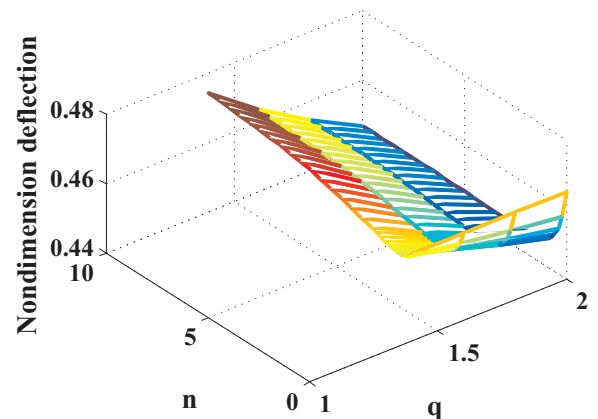
Fig. 3. The effective Young's modulus as a function of n and q .



(a)



(a)



(b)

Fig. 5. Effect of volume fraction coefficients on normalized deflection of a 2D-FGM plate.

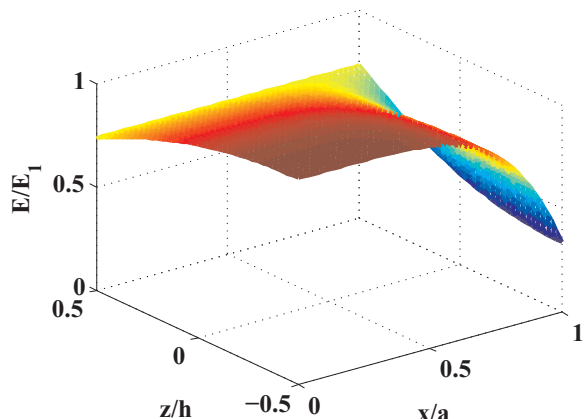
3. Finite element formulation for bending and buckling analysis of 2D-FGM plates

A finite element formulation based on a new third-order shear deformation plate theory, which is originally proposed by Shi in [34], for bending and buckling analysis of 2D-FGM plates is derived in this section. This new plate theory, in which the kinematic of displacements is derived from an elasticity formulation rather than the hypothesis of displacements, has shown more accurate than other higher-order shear deformation plate theories. The displacements, u , v and w at any point of the plate are given by [34]

$$\begin{aligned}
 u(x, y, z) &= u_0(x, y) + \frac{5}{4} \left(z - \frac{4}{3h^2} z^3 \right) \phi_x(x, y) + \left(\frac{1}{4} z - \frac{5}{3h^2} z^3 \right) w_{0,x} \\
 v(x, y, z) &= v_0(x, y) + \frac{5}{4} \left(z - \frac{4}{3h^2} z^3 \right) \phi_y(x, y) + \left(\frac{1}{4} z - \frac{5}{3h^2} z^3 \right) w_{0,y} \\
 w(x, y, z) &= w_0(x, y)
 \end{aligned}
 \tag{3}$$

where u_0 , v_0 , and w_0 are respectively the displacements in the x , y , and z directions of a point on the mid-plane of a plate, while ϕ_x and ϕ_y denote the transverse rotations of a mid-surface normal around the x and y axes, respectively. In Eq. (3) and hereafter, a subscript comma denotes the differentiation with respect to the following x or y coordinate variable.

Under small strain assumptions, the normal and shear strains resulted from Eq. (3) are as follows



(b)

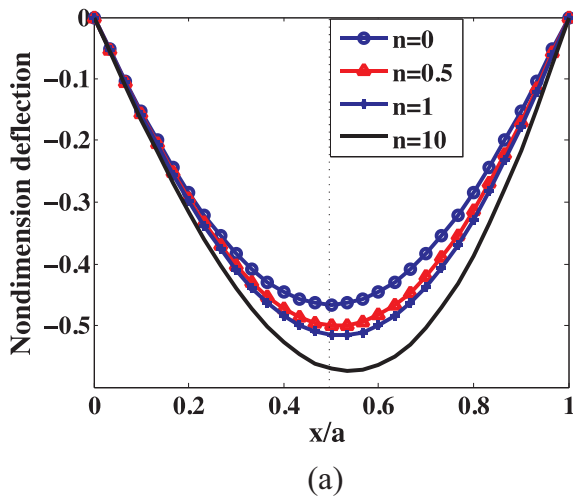
Fig. 4. Distribution of elasticity modulus of the 2D-FGM plate for specific values of volume fraction coefficients, for instance, $n = 2$, $q = 5$ (a) and $n = 0.5$, $q = 0.5$ (b).

The variation of effective Young's modulus E and Poisson's ratio ν in the thickness and longitudinal directions based on this model is as follows

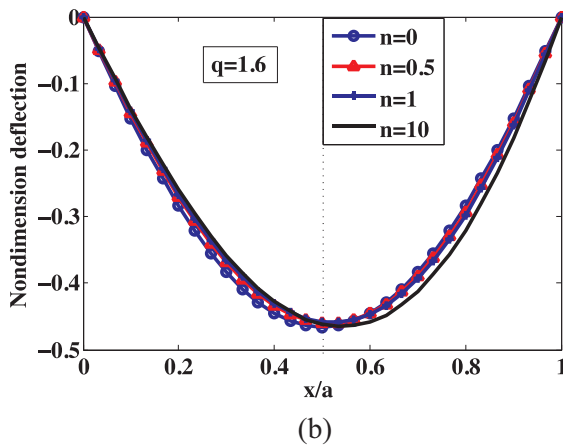
$$\begin{aligned}
 E(x, z) &= E_1 V_1 + E_2 V_2 + E_3 V_3 \\
 \nu(x, z) &= \nu_1 V_1 + \nu_2 V_2 + \nu_3 V_3
 \end{aligned}
 \tag{2}$$

where E_i , ν_i ($i = 1..3$) are Young's modulus and Poisson's ratio of the constituent materials, respectively.

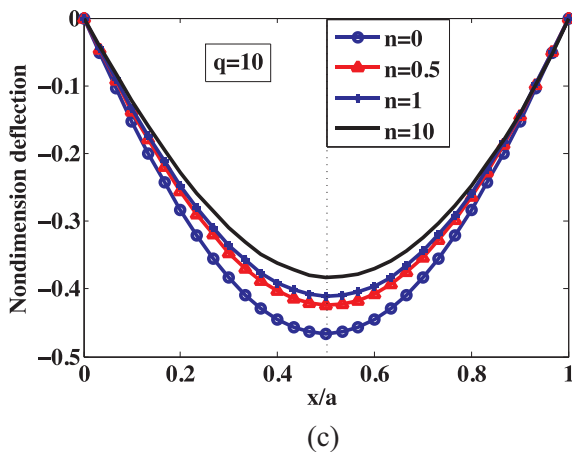
$$\begin{Bmatrix} \varepsilon_x \\ \varepsilon_y \\ \varepsilon_{xy} \\ \gamma_{yz} \\ \gamma_{xz} \end{Bmatrix} = \begin{Bmatrix} u_{0,x} + z\frac{1}{4}(5\phi_{x,x} + w_{,xx}) + z^3\left(\frac{-5}{3h^2}\right)(\phi_{x,x} + w_{,xx}) \\ v_{0,y} + z\frac{1}{4}(5\phi_{y,y} + w_{,yy}) + z^3\left(\frac{-5}{3h^2}\right)(\phi_{y,y} + w_{,yy}) \\ u_{0,y} + v_{0,x} + z\frac{1}{4}(5\phi_{x,y} + 2w_{,xy} + 5\phi_{y,x}) + z^3\left(\frac{-5}{3h^2}\right)(\phi_{x,y} + 2w_{,xy} + \phi_{y,x}) \\ \frac{5}{4}(\phi_y + w_{,y}) + z^2\left(\frac{-5}{h^2}\right)(\phi_y + w_{,y}) \\ \frac{5}{4}(\phi_x + w_{,x}) + z^2\left(\frac{-5}{h^2}\right)(\phi_x + w_{,x}) \end{Bmatrix} \quad (4)$$



(a)

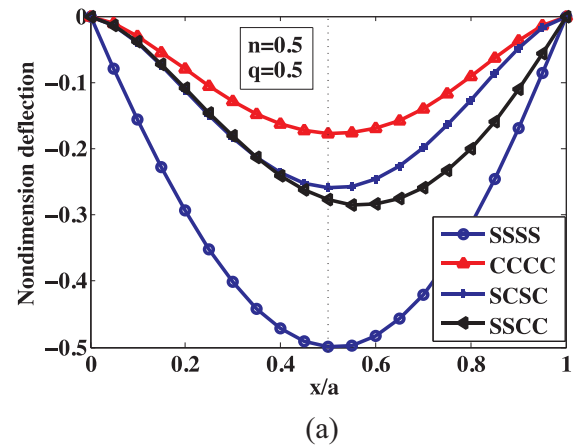


(b)

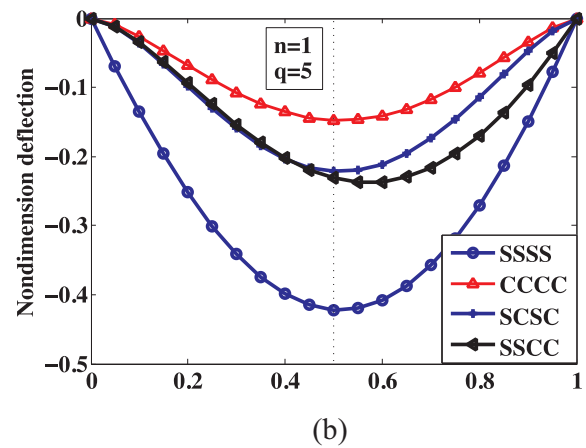


(c)

Fig. 6. Effect of volume fraction coefficients on normalized deflection of a 2D-FGM plate for three specific values of $q=0.5$ (a); $q=1.6$ (b); and $q=10$ (c).



(a)



(b)

Fig. 7. Effects of boundary conditions on normalized deflections of a 2D FGM plate.

Eq. (4) can be rewritten in the matrix form as

$$\begin{Bmatrix} \varepsilon \\ \gamma \end{Bmatrix} = \begin{Bmatrix} \varepsilon^{(0)} \\ \gamma^{(0)} \end{Bmatrix} + z \begin{Bmatrix} \varepsilon^{(1)} \\ 0 \end{Bmatrix} + z^2 \begin{Bmatrix} 0 \\ \gamma^{(2)} \end{Bmatrix} + z^3 \begin{Bmatrix} \varepsilon^{(3)} \\ 0 \end{Bmatrix} \quad (5)$$

in which

$$\begin{aligned} \varepsilon^{(0)} &= \begin{Bmatrix} u_{0,x} \\ v_{0,y} \\ u_{0,y} + v_{0,x} \end{Bmatrix}; \\ \varepsilon^{(1)} &= \frac{1}{4} \begin{Bmatrix} (5\phi_{x,x} + w_{,xx}) \\ (5\phi_{y,y} + w_{,yy}) \\ (5\phi_{x,y} + 2w_{,xy} + 5\phi_{y,x}) \end{Bmatrix}; \\ \varepsilon^{(3)} &= \begin{Bmatrix} \phi_{x,x} + w_{,xx} \\ \phi_{y,y} + w_{,yy} \\ \phi_{x,y} + 2w_{,xy} + \phi_{y,x} \end{Bmatrix} \end{aligned} \quad (6)$$

$$\gamma^{(0)} = \frac{5}{4} \begin{Bmatrix} \phi_y + w_{,y} \\ \phi_x + w_{,x} \end{Bmatrix}; \quad \gamma^{(2)} = \frac{-5}{h^2} \begin{Bmatrix} \phi_y + w_{,y} \\ \phi_x + w_{,x} \end{Bmatrix} \quad (7)$$

Based on Hooke's law, the vectors of normal and shear stresses read

$$\begin{aligned} \sigma &= \mathbf{D}_m(x, z)(\varepsilon^{(0)} + z\varepsilon^{(1)} + z^3\varepsilon^{(3)}) \\ \tau &= \mathbf{D}_s(x, z)(\gamma^{(0)} + z^2\gamma^{(2)}) \end{aligned} \quad (8)$$

where

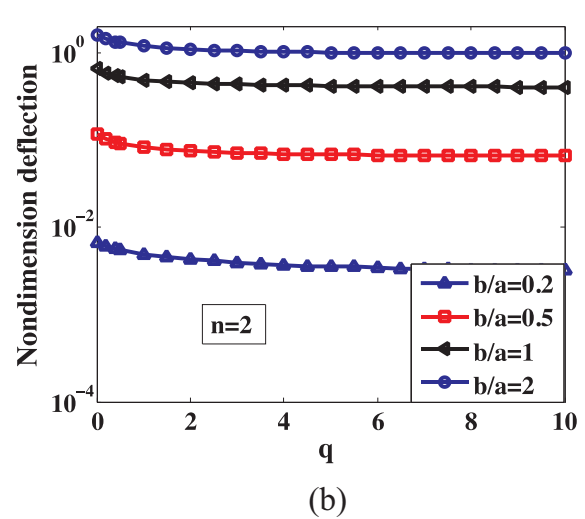
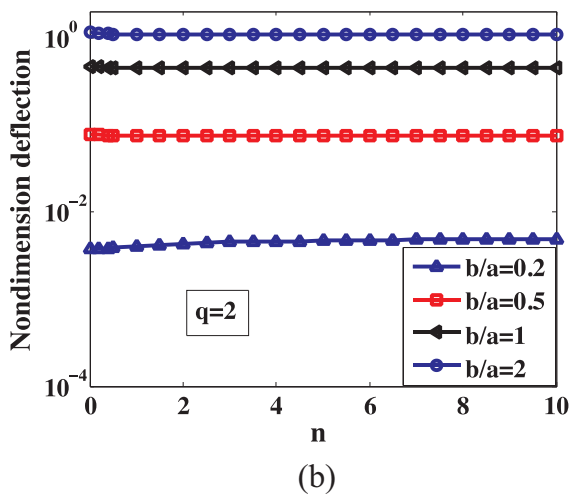
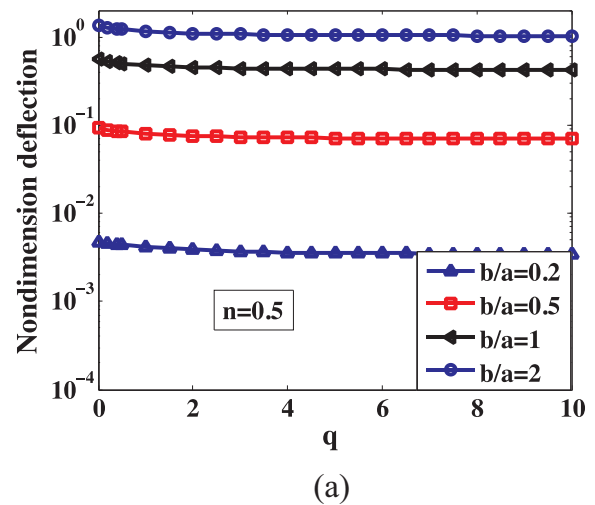
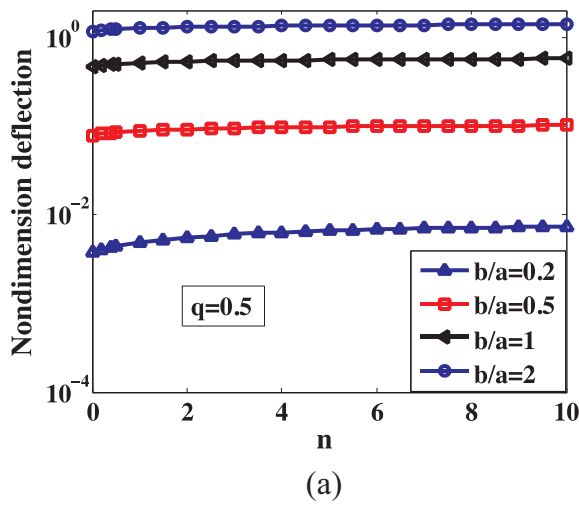


Fig. 8. Effect of width-to-length ratio b/a on normalized deflection of a 2D-FGM plate.

Fig. 9. Effect of width-to-length ratio b/a on normalized deflection of a 2D-FGM plate.

$$\sigma = [\sigma_x \ \sigma_y \ \sigma_{xy}]^T; \ \tau = [\tau_{yz} \ \tau_{xz}]^T \tag{9a}$$

$$\mathbf{D}_m(x, z) = \frac{E}{1 - \nu^2} \begin{bmatrix} 1 & \nu & 0 \\ \nu & 1 & 0 \\ 0 & 0 & (1 - \nu)/2 \end{bmatrix} \tag{9b}$$

$$\mathbf{D}_s(x, z) = \frac{E}{2(1 + \nu)} \begin{bmatrix} 1 & 0 \\ 0 & 1 \end{bmatrix} \tag{9c}$$

with E and ν are respectively the effective Young's modulus and Poisson's ratio defined by Eq. (2), which are functions of both the x and z coordinates for the 2D-FGM plate considered herein.

A quadrilateral 4-node plate element, in which each node contains seven degrees of freedom, namely $\mathbf{q}_i = \{u_{0i} \ v_{0i} \ w_i \ \phi_{xi} \ \phi_{yi} \ \frac{\partial w}{\partial x} \ \frac{\partial w}{\partial y}\}^T$, $i = 1 - 4$ is considered. The displacements and rotations inside the element are interpolated from the nodal values according to

$$\begin{aligned} & [u_0, v_0, \phi_x, \phi_y]^T \\ & = [\sum_{i=1}^4 N_i, u_{0i}, \dots, \sum_{i=1}^4 N_i, v_{0i}, \dots, \sum_{i=1}^4 N_i, \phi_{xi}, \dots, \sum_{i=1}^4 N_i, \phi_{yi}]^T \\ w & = H_1 w_{01} + H_2 \left(\frac{\partial w}{\partial x}\right)_1 + H_3 \left(\frac{\partial w}{\partial y}\right)_1 + \dots + H_{10} w_{04} + H_{11} \left(\frac{\partial w}{\partial x}\right)_4 \\ & + H_{12} \left(\frac{\partial w}{\partial y}\right)_4 \end{aligned} \tag{10}$$

where N_i and H_i denote the interpolation functions. In the present work, Lagrange and Hermite polynomials are adopted for N_i and H_i , respectively.

The interpolation scheme (10) can be written in the matrix form as

$$\mathbf{u}_0 = \mathbf{B}_H \mathbf{q}_e \tag{11a}$$

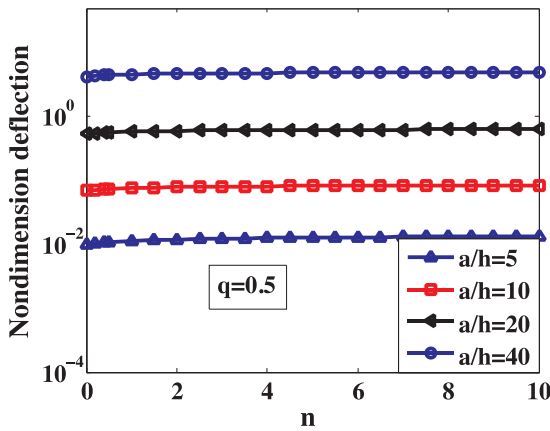
with \mathbf{B}_H denotes the matrix of interpolation functions, and

$$\begin{aligned} \mathbf{u}_0 & = [u_0, v_0, w_0, \phi_x, \phi_y, w_{,x}, w_{,y}]^T \\ \mathbf{q}_e & = [\mathbf{q}_{1e} \ \mathbf{q}_{2e} \ \mathbf{q}_{3e} \ \mathbf{q}_{4e}]^T \end{aligned} \tag{11b}$$

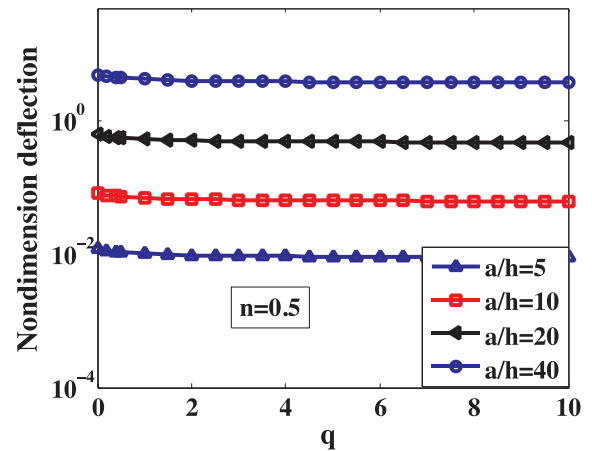
are the vectors of independent variables and nodal values, respectively. By substituting Eq. (11) into Eqs. (6) and (7), the strains can be obtained as follows

$$\begin{aligned} \varepsilon & = (\mathbf{B}_1 + \mathbf{B}_2 + \mathbf{B}_3) \mathbf{q}_e; \\ \gamma & = (\mathbf{B}_4 + \mathbf{B}_5) \mathbf{q}_e \end{aligned} \tag{12}$$

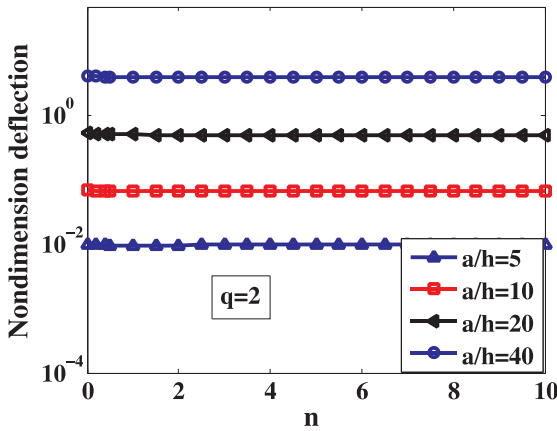
with



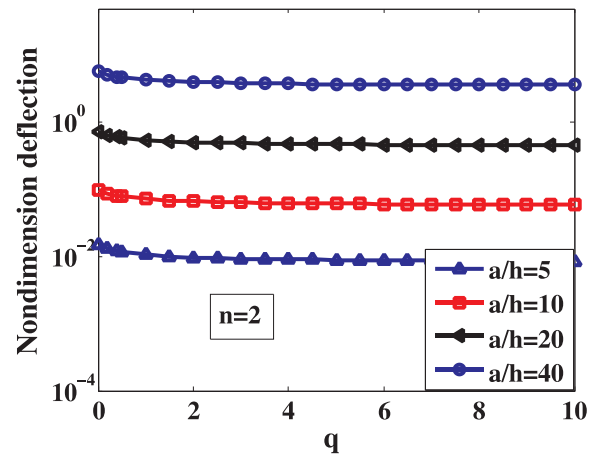
(a)



(a)



(b)



(b)

Fig. 10. Effect of plate thickness on normalized deflection of the 2D-FGM plate.

Fig. 11. Effect of plate thickness on normalized deflection of the 2D-FGM plate.

$$\begin{aligned}
 \mathbf{B}_1 &= \sum_i^4 \begin{bmatrix} N_{i,x} & 0 & 0 & 0 & 0 \\ 0 & N_{i,y} & 0 & 0 & 0 \\ N_{i,y} & N_{i,x} & 0 & 0 & 0 \end{bmatrix}; \\
 \mathbf{B}_2 &= \frac{1}{4} \sum_{i=1}^4 \begin{bmatrix} 0 & 0 & (H_{(3i-2),x})_x & 5N_{i,x} & 0 & (H_{(3i-1),x})_x & (H_{(3i),x})_x \\ 0 & 0 & (H_{(3i-2),y})_y & 0 & 5N_{i,y} & (H_{(3i-1),y})_y & (H_{(3i),y})_y \\ 0 & 0 & 2(H_{(3i-2),x})_y & 5N_{i,y} & 5N_{i,x} & 2(H_{(3i-1),x})_y & 2(H_{(3i),x})_y \end{bmatrix}; \\
 \mathbf{B}_3 &= -\frac{5}{3h^2} \sum_{i=1}^4 \begin{bmatrix} 0 & 0 & (H_{(3i-2),x})_x & N_{i,x} & 0 & (H_{(3i-1),x})_x & (H_{(3i),x})_x \\ 0 & 0 & (H_{(3i-2),y})_y & 0 & N_{i,y} & (H_{(3i-1),y})_y & (H_{(3i),y})_y \\ 0 & 0 & 2(H_{(3i-2),x})_y & N_{i,y} & N_{i,x} & 2(H_{(3i-1),x})_y & 2(H_{(3i),x})_y \end{bmatrix}
 \end{aligned}
 \tag{13a}$$

and

$$\begin{aligned}
 \mathbf{B}_4 &= \frac{5}{4} \sum_{i=1}^4 \begin{bmatrix} 0 & 0 & H_{(3i-2),x} & N_i & 0 & H_{(3i-1),x} & H_{3i,x} \\ 0 & 0 & H_{(3i-2),y} & 0 & N_i & H_{(3i-1),y} & H_{3i,y} \end{bmatrix}; \\
 \mathbf{B}_5 &= -\frac{5}{h^2} \begin{bmatrix} 0 & 0 & H_{(3i-2),x} & N_i & 0 & H_{(3i-1),x} & H_{3i,x} \\ 0 & 0 & H_{(3i-2),y} & 0 & N_i & H_{(3i-1),y} & H_{3i,y} \end{bmatrix}
 \end{aligned}
 \tag{13b}$$

The normal forces, bending moments, higher-order moments and shear force can then be computed through the following relations

$$\begin{aligned}
 \tilde{\mathbf{N}} &= \{\tilde{N}_x \tilde{N}_y \tilde{N}_{xy}\}^T \\
 &= \int_{-h/2}^{h/2} \{\sigma_x \sigma_y \sigma_{xy}\}^T dz \\
 &= \int_{-h/2}^{h/2} \mathbf{D}_m(x, z) (\boldsymbol{\varepsilon}^{(0)} + z\boldsymbol{\varepsilon}^{(1)} + z^3\boldsymbol{\varepsilon}^{(3)}) dz
 \end{aligned}
 \tag{14a}$$

$$\begin{aligned}
 \tilde{\mathbf{M}} &= \{\tilde{M}_x \tilde{M}_y \tilde{M}_{xy}\}^T \\
 &= \int_{-h/2}^{h/2} \{\sigma_x \sigma_y \sigma_{xy}\}^T z dz \\
 &= \int_{-h/2}^{h/2} \mathbf{D}_m(x, z) (\boldsymbol{\varepsilon}^{(0)} + z\boldsymbol{\varepsilon}^{(1)} + z^3\boldsymbol{\varepsilon}^{(3)}) z dz
 \end{aligned}
 \tag{14b}$$

$$\begin{aligned}
 \tilde{\mathbf{P}} &= \{\tilde{P}_x \tilde{P}_y \tilde{P}_{xy}\}^T \\
 &= \int_{-h/2}^{h/2} \{\sigma_x \sigma_y \sigma_{xy}\}^T z^3 dz \\
 &= \int_{-h/2}^{h/2} \mathbf{D}_m(x, z) (\boldsymbol{\varepsilon}^{(0)} + z\boldsymbol{\varepsilon}^{(1)} + z^3\boldsymbol{\varepsilon}^{(3)}) z^3 dz
 \end{aligned}
 \tag{14c}$$

$$\tilde{\mathbf{Q}} = \{\tilde{Q}_y \tilde{Q}_x\}^T = \int_{-h/2}^{h/2} \{\tau_{yz} \tau_{xz}\}^T dz = \int_{-h/2}^{h/2} \mathbf{D}_s(x, z) (\boldsymbol{\gamma}^{(0)} + z^2\boldsymbol{\gamma}^{(2)}) dz
 \tag{14d}$$

$$\tilde{\mathbf{R}} = \{\tilde{R}_y \tilde{R}_x\}^T = \int_{-h/2}^{h/2} \{\tau_{yz} \tau_{xz}\}^T z^2 dz = \int_{-h/2}^{h/2} \mathbf{D}_s(x, z) (\boldsymbol{\gamma}^{(0)} + z^2\boldsymbol{\gamma}^{(2)}) z^2 dz
 \tag{14e}$$

Eq. (14) can be recast in matrix form as follows

$$\begin{bmatrix} \tilde{\mathbf{N}} \\ \tilde{\mathbf{M}} \\ \tilde{\mathbf{P}} \\ \tilde{\mathbf{Q}} \\ \tilde{\mathbf{R}} \end{bmatrix} = \begin{bmatrix} \mathbf{A} & \mathbf{B} & \mathbf{E} & \mathbf{0} & \mathbf{0} \\ \mathbf{B} & \mathbf{D} & \mathbf{F} & \mathbf{0} & \mathbf{0} \\ \mathbf{E} & \mathbf{F} & \mathbf{H} & \mathbf{0} & \mathbf{0} \\ \mathbf{0} & \mathbf{0} & \mathbf{0} & \hat{\mathbf{A}} & \hat{\mathbf{B}} \\ \mathbf{0} & \mathbf{0} & \mathbf{0} & \hat{\mathbf{B}} & \hat{\mathbf{D}} \end{bmatrix} \begin{bmatrix} \boldsymbol{\varepsilon}^{(0)} \\ \boldsymbol{\varepsilon}^{(1)} \\ \boldsymbol{\varepsilon}^{(3)} \\ \boldsymbol{\gamma}^{(0)} \\ \boldsymbol{\gamma}^{(2)} \end{bmatrix}
 \tag{15}$$

with

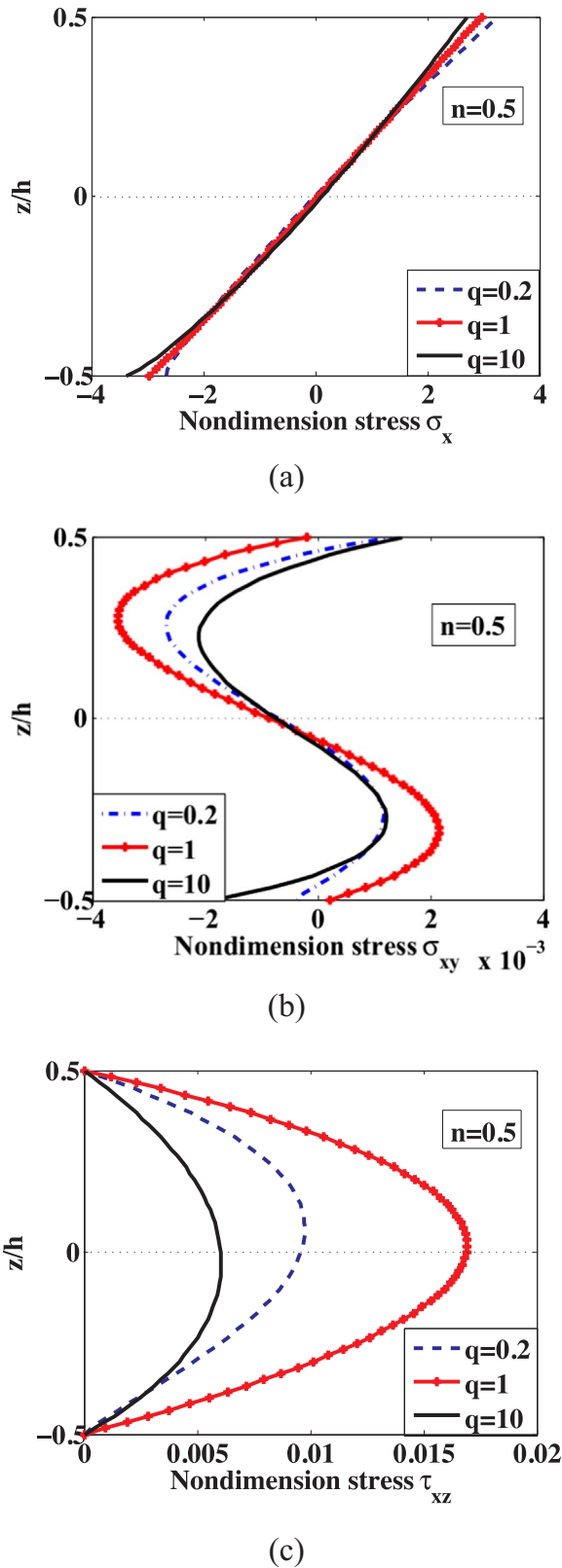


Fig. 12. Distribution of stresses along the plate thickness of a SSSS 2D FGM plate.

$$(A, B, D, E, F, H) = \int_{-h/2}^{h/2} (1, z, z^2, z^3, z^4, z^6) \mathbf{D}_m(x, z) dz \quad (16a)$$

$$(\hat{A}, \hat{B}, \hat{D}) = \int_{-h/2}^{h/2} (1, z^2, z^4) \mathbf{D}_s(x, z) dz \quad (16b)$$

Table 3

Comparison of the critical buckling load (MN/m) for a square SSSS 1D-FGM plate ($a = b = 1$ m, $h = a/100$, $q = 0$).

Buckling load	$n = 0$	$n = 1$	$n = 2$
Meisam [14] (Analytical)	1.3737	0.6847	0.5343
Bodaghi [13] (Analytical)	1.3730	0.6844	0.5340
This work	1.3722	0.6835	0.5331

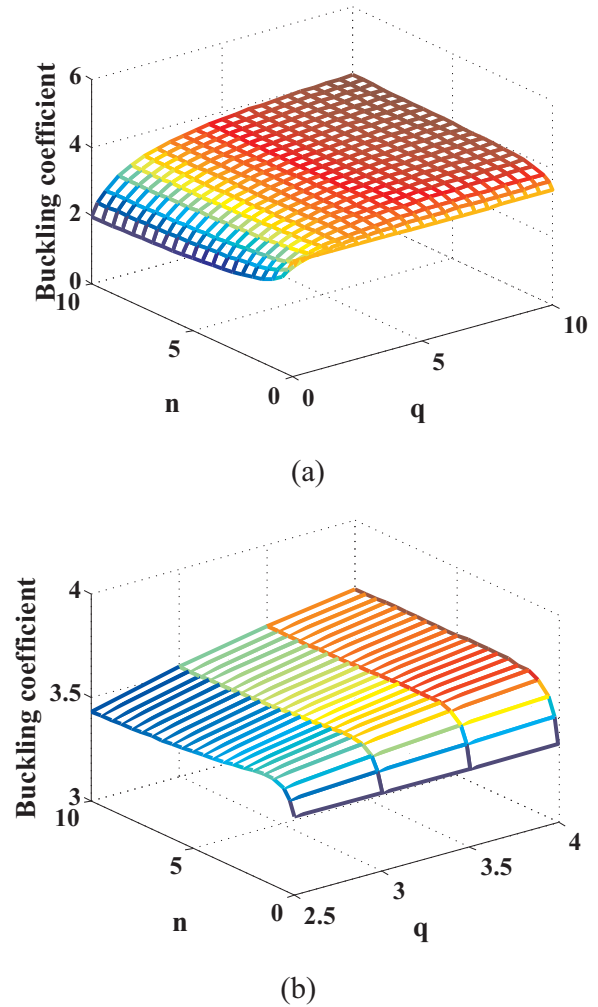


Fig. 13. The critical buckling load as a function of volume fraction coefficients of a 2D-FGM plate obtained by the developed method.

The total strain energy of a plate due to the normal forces, shear force, bending moments and higher-order moments can be given by

$$U = \frac{1}{2} \int_{V_e} \boldsymbol{\varepsilon}^T \boldsymbol{\sigma} dV - \int_{S_e} \mathbf{u}^T \mathbf{f} dS$$

$$= \frac{1}{2} \mathbf{q}_e^T \int_{S_e} \left(\begin{array}{l} \mathbf{B}_1^T \mathbf{A} \mathbf{B}_1 + \mathbf{B}_1^T \mathbf{B} \mathbf{B}_2 + \mathbf{B}_1^T \mathbf{E} \mathbf{B}_3 + \\ + \mathbf{B}_2^T \mathbf{B} \mathbf{B}_1 + \mathbf{B}_2^T \mathbf{D} \mathbf{B}_2 + \mathbf{B}_2^T \mathbf{F} \mathbf{B}_3 + \\ + \mathbf{B}_3^T \mathbf{E} \mathbf{B}_1 + \mathbf{B}_3^T \mathbf{F} \mathbf{B}_2 + \mathbf{B}_3^T \mathbf{H} \mathbf{B}_3 + \\ + \mathbf{B}_4^T \hat{\mathbf{A}} \mathbf{B}_4 + \mathbf{B}_4^T \hat{\mathbf{B}} \mathbf{B}_5 + \mathbf{B}_5^T \hat{\mathbf{B}} \mathbf{B}_4 + \\ + \mathbf{B}_5^T \hat{\mathbf{D}} \mathbf{B}_5 \end{array} \right) dS \mathbf{q}_e - \mathbf{q}_e^T \int_{S_e} \mathbf{B}_H^T \mathbf{f} dS \quad (17)$$

where \mathbf{f} is the transverse loading per unit area, and Eq. (17) can be rewritten in matrix form as

$$U = \frac{1}{2} \mathbf{q}_e^T \mathbf{K}_e \mathbf{q}_e - \mathbf{q}_e^T \mathbf{F}_e \quad (18a)$$

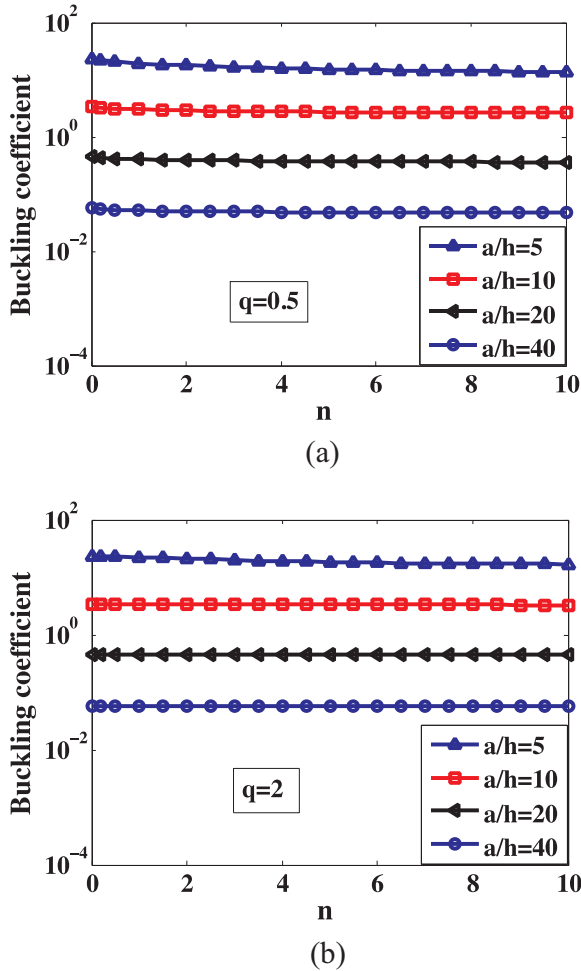


Fig. 14. The effect of the plate thickness on the critical buckling load for a 2D-FGM plate.

$$U = \mathbf{q}_e^T \left(\frac{1}{2} \mathbf{K}_e \mathbf{q}_e - \mathbf{F}_e \right) \tag{18b}$$

with \mathbf{K}_e in Eq. (18) being the element stiffness matrix, whilst \mathbf{F}_e representing the element force vector.

For bending analysis, the bending solutions can be obtained by solving the following equation

$$\mathbf{K} \mathbf{d} = \mathbf{F} \tag{19}$$

where \mathbf{K} and \mathbf{F} are respectively the global stiffness matrix and force vector, while \mathbf{d} stands for the vector of unknowns nodal displacements.

The membrane strains associated with the lateral displacement and rotations in the case of the plate subjected to in-plane pre-buckling stresses are given by

$$\boldsymbol{\varepsilon}_P^G = \begin{bmatrix} \frac{1}{2} \left(\frac{\partial w}{\partial x} \right)^2 + \frac{z^2}{2} \left(\frac{\partial \phi_x}{\partial x} \right)^2 + \frac{z^2}{2} \left(\frac{\partial \phi_y}{\partial x} \right)^2 \\ \frac{1}{2} \left(\frac{\partial w}{\partial y} \right)^2 + \frac{z^2}{2} \left(\frac{\partial \phi_x}{\partial y} \right)^2 + \frac{z^2}{2} \left(\frac{\partial \phi_y}{\partial y} \right)^2 \\ \frac{\partial w}{\partial x} \frac{\partial w}{\partial y} + z^2 \frac{\partial \phi_x}{\partial x} \frac{\partial \phi_x}{\partial y} + z^2 \frac{\partial \phi_y}{\partial x} \frac{\partial \phi_y}{\partial y} \\ 0 \\ 0 \end{bmatrix} \tag{20}$$

The geometric strain energy enforced by in-plane pre-buckling stresses is then computed by

$$U^G = \frac{1}{2} \sum_{V_e} \int_{V_e} \hat{\boldsymbol{\sigma}}_0^T \boldsymbol{\varepsilon}_P^G dV \tag{21a}$$

with

$$\hat{\boldsymbol{\sigma}}_0^T = [\sigma_x^0, \sigma_y^0, \tau_{xy}^0, 0, 0]^T \tag{21b}$$

By substituting the membrane strains of the plate in to Eq. (21) and integrating on the thickness of the plate, the geometric strain energy become

$$U^G = \frac{1}{2} \sum_{S_e} \int_{S_e} (\boldsymbol{\varepsilon}_P^G)^T \boldsymbol{\sigma}_0 \boldsymbol{\varepsilon}_P^G dS \tag{22}$$

where

$$\boldsymbol{\varepsilon}_P^G = \begin{Bmatrix} w_{,x} \\ w_{,y} \\ \phi_{x,x} \\ \phi_{x,y} \\ \phi_{y,x} \\ \phi_{y,y} \end{Bmatrix} = \begin{bmatrix} 0 & 0 & 0 & 0 & 0 & 1 & 0 \\ 0 & 0 & 0 & 0 & 0 & 0 & 1 \\ 0 & 0 & 0 & \frac{\partial}{\partial x} & 0 & 0 & 0 \\ 0 & 0 & 0 & \frac{\partial}{\partial y} & 0 & 0 & 0 \\ 0 & 0 & 0 & 0 & \frac{\partial}{\partial x} & 0 & 0 \\ 0 & 0 & 0 & 0 & \frac{\partial}{\partial y} & 0 & 0 \end{bmatrix} \begin{Bmatrix} u \\ v \\ w \\ \phi_x \\ \phi_y \\ w_{,x} \\ w_{,y} \end{Bmatrix} = \mathbf{L}_P^G \mathbf{q}_e \tag{23}$$

$$\boldsymbol{\sigma}_0 = \text{diag} \left(h \bar{\sigma}, \frac{h^3}{12} \bar{\sigma}, \frac{h^3}{12} \bar{\sigma} \right); \quad \bar{\boldsymbol{\sigma}} = [\sigma_x^0, \tau_{xy}^0, \sigma_y^0] \tag{24}$$

Expressing Eq. (21) in matrix form

$$U^G = \frac{1}{2} \sum_{N_p} \mathbf{q}_e^T \mathbf{K}_e^G \mathbf{q}_e \tag{25}$$

The equation for pre-buckling analysis of the 2D-FGM plate in the finite element analysis reads

$$\{\mathbf{K} - \lambda_b \mathbf{K}^G\} \mathbf{d} = 0 \tag{26}$$

where λ_b is a loading parameter. Eq. (26) is an eigenvalue problem, whose smallest root

defines the smallest level of external load for which the plate is buckle or bifurcation.

4. Numerical results and discussion

In this section, numerical solutions for bending static deflection and buckling of 2D-FGM plates computed by using the proposed approach with the new third-order shear deformation theory are presented and discussed. The 2D-FGM plates under both the simply supported and fully clamped boundary conditions are considered and investigated. In the numerical examples, for the simply supported plates the boundary conditions are set as

$$v_0 = w = \phi_y = 0, \text{ at } x = 0, a \tag{27a}$$

$$u_0 = w = \phi_x = 0, \text{ at } y = 0, b \tag{27b}$$

while the fully clamped edges

$$u_0 = v_0 = w = \phi_x = \phi_y = \partial w / \partial x = \partial w / \partial y = 0, \text{ at } x = 0, a \text{ and } y = 0, b \tag{28}$$

4.1. Accuracy analysis

This analysis is to show the accuracy of the developed formulation. We validate by comparing the computed deflections and stresses with respect to reference solutions available in the literature. A fully simply supported Al/Al₂O₃ plate ($a/b = 1$ and $a/h = 10$) subjected to a uniform load P is considered. The material parameters of Al and Al₂O₃, $\nu_m = 0.3$, $E_m = 70GPa$, and are $\nu_c = 0.3$, $E_c = 380GPa$, respectively, are used for the investigation. We assume that the Al/Al₂O₃ material adopted is to be independent of temperature. In this analysis, the maximum central deflection and normal stress are normalized by

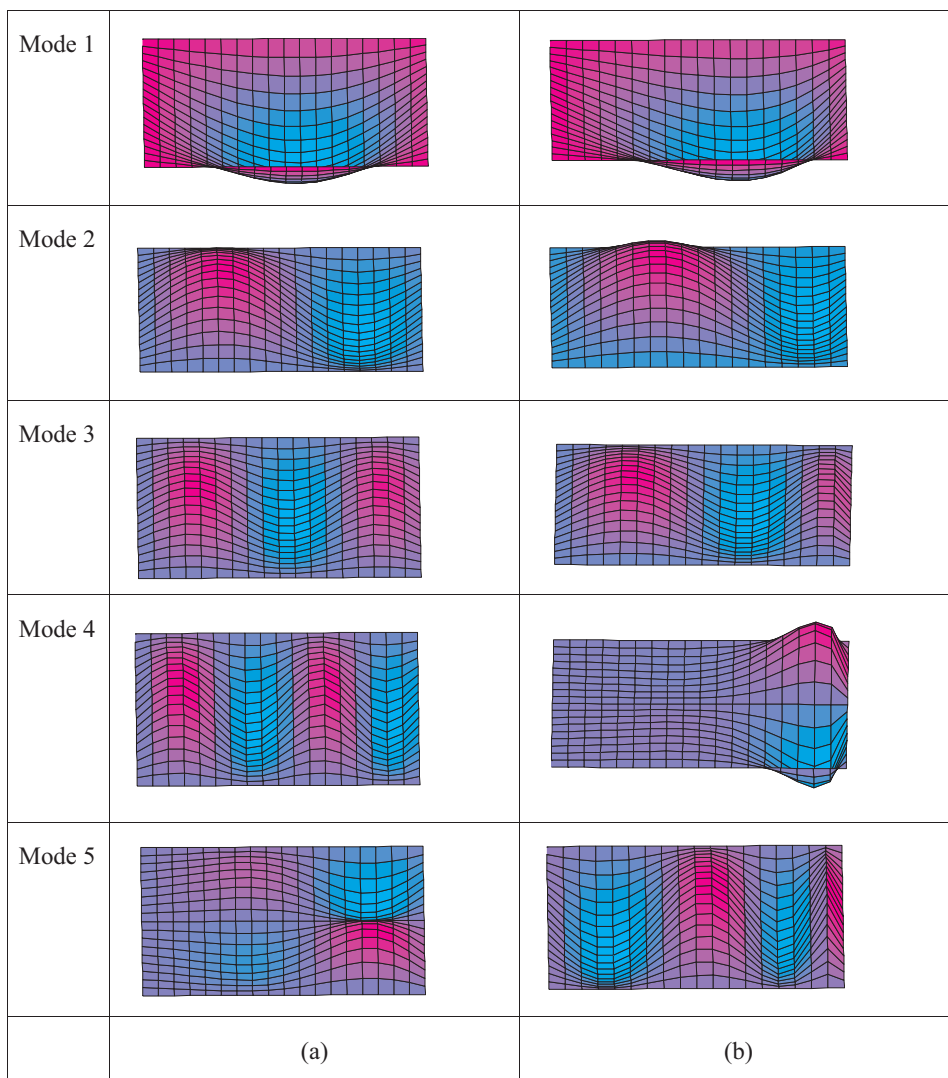


Fig. 15. The first five buckling mode-shapes of 2D-FGM plates, (a): $n = 0.5, q = 0.5$ and (b): $n = 10, q = 1$.

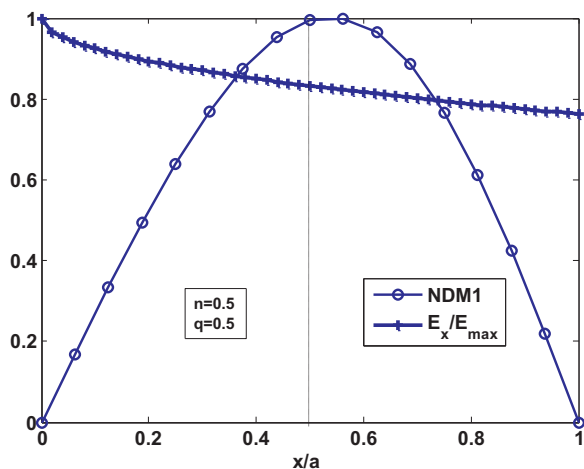


Fig. 16. The correlation of critical buckling load and Young's modulus of a 2D FGM plate.

$$\begin{aligned} \bar{w} &= \frac{10h^3 E_c}{Pa^4} w\left(\frac{a}{2}, \frac{b}{2}\right) \\ \bar{\sigma}_{xx} &= \frac{h}{Pa} \sigma_{xx}\left(\frac{a}{2}, \frac{b}{2}, \frac{h}{2}\right) \end{aligned} \quad (29)$$

The developed FEM method is applied to solve the defined problem

of a simply supported one-directional FGM (1D-FGM) square plate, and the computed normalized deflections and tensile stress are reported in Table 1. In Table 1, solutions derived from other theories such as the Reddy's theory [3], the sinusoidal shear deformation plate theory (SSDPT) [4], and the high shear deformation theory (HSDT) [10] are also added for the comparison purpose. Results for different volume fractions such as a pure ceramic ($n = 0$), a pure metal ($n = \infty$), and $n = 1, 2, 3, 5,$ and 10 are also reported. One must be noticed that another coefficient q defined in Section 2 is set to be zero in this analysis. Clearly, the present approach offers a good agreement of deflections and stresses with the reference theories.

4.2. Static bending analysis of 2D-FGM plates

A 2D-FGM plate made from three materials with properties listed in Table 2 is considered. The 2D-FGM plate is subjected to a uniform load P , and its deflection and stress are computed by the derived formulation. A parametric study for some relevant parameters is also carried out. The dimensionless parameters for the deflection and stress defined by Eq. (29) are employed again herewith.

The effective Young's modulus in terms of 2D-FGM depends upon the three individual materials is determined by the following expression:

$$E_{eff} = \frac{\int_V (E_1 V_1 + E_2 V_2 + E_3 V_3) dV}{V} \tag{30}$$

The effective Young's modulus of 2D-FGM plates whose material properties listed in Table 2 is also depicted in Fig. 3 (from Eq. (30)). In addition, Fig. 4a and b show the distribution of elastic module (E) through x and z axes of 2D FGM plate for particular cases of $n = 2, q = 5$ and $n = 0.5, q = 0.5$ (from Eq. (2a)).

4.2.1. Effect of volume fractions

A fully simple supported 2D-FGM plate with geometry $a/b = 1$ and $a/h = 10$ is considered. The deflection of 2D FGM plate computed by using the present method dependent on the volume fraction coefficients is plotted in Fig. 5. In that result, the volume fraction parameters n and q varying from 0 to 10 are considered. In general, the volume fraction coefficients have a significant influence on the deflection in some range. For instance, they greatly alter the deflection only for the volume fractions n and p are in range of 0–2 (see Fig. 5), whereas there are insignificant or slight effects.

Unlike 1D-FGM plates, the mechanical behaviors of 2D-FGM plates are more complicated. The variation of volume fraction coefficients in the 2D-FGM plates n and q greatly alters the normalized deflections. The dependence of mechanical behaviors of plates on the volume fraction coefficients n and q in Fig. 5 is clear when examining the variation of the effective Young's modulus with these coefficients, which is depicted in Fig. 3. In addition, the normalized deflection (see Fig. 5) reaches the maximum once the minimum of the effective Young's modulus holds (see Fig. 3).

Fig. 6 depicts the normalized deflection at $y = b/2$ for three specific values of q such as 0.5, 1.6 and 10 while n takes from 0 to 10. We can see again in Fig. 6 that the volume fraction factors q and n have strong effects on the mechanical behaviors of 2D FGM plates. The second volume fraction coefficient q , which defines the variation of the material properties in the longitudinal direction, has significant influence on the deflection of the plate, and as clearly seen from Fig. 6(a), the deflection of the 2D-plate is unsymmetrical with respect to the middle line $x = a/2$ as in case of the 1D-FGM plate. The maximum deflection for each case of q is different from each other, and it decreases with the increase of the coefficient q . At a given value of the coefficient n , the effective elastic modulus of the 2D-FGM plate, as seen from Fig. 3, increases by increasing the coefficient q , and this can be explained for the decrease of the deflection by the increase of the coefficient q . Moreover, the effect of the coefficient n , which defines the variation of the plate properties on in the thickness direction, on the deflection of the 2D-FGM plate, as seen from the figure, is dependent on the value of the second coefficient q . For $q = 0.5$, Fig. 6(a) shows an increase in the deflection by increasing n , but for $q = 10$, as can be seen from Fig. 6(c), the deflection decrease by the increase of the coefficient n .

Additionally, the influence of the boundary conditions on the mechanical deflection of a 2D-FGM plate is explored. Fig. 7 shows the plate deflection lines at $y = b/2$ with four boundary conditions (SSSS, CCCC, SCSC and SSCC) and two couples of the volume fraction factors, e.g., $n = q = 0.5$ and $n = 1, q = 5$. Large effects of the boundary conditions on the normalized deflections are obtained. The numerical results presented are consistent as the CCCC plate in comparison with other considered plates obtains the smallest deflection.

4.2.2. Effect of width-to-length ratio b/a

We now analyze the effect of the aspect ratio a/b on the mechanical behavior of a fully simple supported 2D-FGM plate. The length of plate a is assumed to be constant, while the plate thickness $h = a/10$, and b/a varies from 0.2 to 4.

Figs. 8 and 9, respectively, show the computed normalized deflections as a function of aspect ratio and two volume fraction factors n and q . Some interesting phenomena can be observing from the figures. The higher the ratio b/a is taken the larger the normalized deflections of

plates are obtained. It implies that the width-to-length ratio b/a strongly alters the mechanical behaviors of the 2D-FGM plate. From these results, we again, once more time, can observe the effects of the volume fraction factors on the mechanical behaviors discussed above, and the dependence of the plate deflection on the factor n much depends on the value of the factor q .

4.2.3. Effect of plate thickness

A SSSS 2D-FGM plate with $a/b = 1$ is considered. The plate thickness h is taken from $a/5$ to $a/50$. The results of the mid-plate deflection as a function of plate thickness and two values of volume fraction factors n and q are shown in Figs. 10 and 11. In this particular analysis, the normalized deflection is redefined by

$$\bar{w} = \frac{w_c E_1}{1000(1 - \nu_1^2) Pa} \tag{31}$$

The main reason to recalculate the normalized deflection in Eq. (31) is to get rid of the plate thickness effect. Similar to the width-to-length ratio above, the plate thickness also has a significant influence on the mechanical deflection of the 2D-FGM plate. As expected, the smaller the plate thickness is taken the larger the mechanical deflections are obtained, regardless of the volume fraction coefficients. More importantly, our own numerical experiments show that the new TSDT used here is free from the shear-locking as the plate thickness gets smaller.

4.2.4. Distribution of stresses in 2D-FGM plates

Fig. 12 shows the distribution of stresses along the plate thickness of a SSSS 2D-FGM plate ($a/b = 1, a/h = 10$) with $n = 0.5$ and three values of $q = 0.5, 1$ and 10. The figure shows a strong influence of the volume fraction coefficient q on the thickness distribution of the normal and shear stresses of the 2D-FGM plate, and the curves for the normal stress are highly nonlinear with the presence of q . As in case of the deflection, the effect of the coefficient q on the normal and shear stresses depends on the value of n , and an increase in q does not lead to an increase of the maximum stresses. As expected, the normal stress σ_x reaches its maximum at the top and bottom surface, while the shear stress τ_{xz} becomes zero at those surfaces. It essentially shows the accuracy of high-order shear Shi's theory about the distribution of shear stress along the plate thickness.

4.3. Buckling analysis of 2D-FGM plates

In this subsection, buckling of 2D-FGM plates is numerically analyzed using the proposed approach. A square SSSS 1D-FGM plate ($a = b = 1$ m) with a thickness $h = a/100$ is firstly considered to verify the accuracy of the present derived TSDT formulation. The material properties of metal and ceramic, $\nu_m = 0.3, E_m = 70$ GPa, and are $\nu_c = 0.3, E_c = 380$ GPa, respectively. This plate is compressed at two opposite edges. Notice that this FGM plate is a special case of 2D-FGM plates when $q = 0$ ($V_1 = 0, \nu_m = \nu_2, E_m = E_2, \nu_c = \nu_3, E_c = E_3$). The present critical buckling results are thus compared with the analytical solutions given by Meisam [14] and Bodaghi [13], which are finally reported in Table 3. Our model offers acceptable results and they are in good agreement with the analytical solutions.

Next, we analyze the critical buckling load for a square SSSS 2D-FGM plate ($a/b = 1, h = a/10$) made of three materials with the properties in Table 2. The buckling coefficient is determined as

$$k_{buk} = \lambda_b \cdot a^2 / (E_3 \cdot h^3) \tag{32}$$

where λ_b is the critical buckling load.

The variation of the volume fraction factors n and q affects the critical buckling load computed by the developed method is shown in Fig. 13. The values of q and n are set to be within the range of 0–10. In Fig. 13, the critical buckling load is as a function of q and n , and its behaviors are generally more complicated than those of 1D-FGM plates. The complicated material properties of the 2D-FGM plate can induce

the complexity of the critical buckling load here, also found for the mechanical deflection above. In the results shown here, we can see the strong effects of the volume fraction factors on the critical buckling load when the value of q is taken from 0 to 2. Again we can observe that the dependence of the buckling behaviors of plates on the volume fraction coefficients n and q is clear, which may also be observing through the effective Young's modulus (see Fig. 3).

The effect of the plate thickness on the critical buckling load for a 2D-FGM plate for two values of $q = 0.5$ and 2 is shown in Fig. 14. This is, again, a square and SSSS 2D-FGM plate. Different values of the plate thickness, e.g., a/h is taken from 5 to 50, are considered. The numerical results shown in Fig. 14 are interesting as the behavior of the buckling load is in contrast to that of the mechanical deflection (see Figs. 10 and 11). The critical buckling load increases with increasing the plate thickness. In each case of q index, the critical buckling load gradually decreases with increasing the volume fraction factor n .

Additionally, the first five buckling modes of the 2D-FGM plate with $n = q = 0.5$ and $n = 10$ and $q = 1$ obtained by the developed method are shown in Fig. 15. The buckling modes reveal not symmetric, which may be affected by the distribution of Young's modulus along x -axis. We may also realize the correlation between the maximum of critical buckling load and the maximum of Young's modulus in x -axis, which is schematically depicted in Fig. 16. In this figure, the results termed as "NDM1" represent the non-dimensional deflection of mode 1 at $y = b/2$, which is determined via the following expression $NDM1 = w(x, b/2)/w_{max}$. One may see that the Young's modulus varies in x -axis, and its maximum of critical buckling of mode 1 is athwart behind the position $x = a/2$, but it tends to the direction at which the Young's modulus is small.

5. Conclusions and outlooks

Static buckling and bending behaviors of 2D-FGM plates, which are of great importance in the design and development of engineering applications, are analyzed. An accurate computational approach based on FEM and a new third-order shear deformation plate theory (TSDT) is thus developed. This new approach of the kinematics of plates does not require any special treatments of the shear-locking effect, and the shear correction factors are not required as well. The present TSDT theory based on rigorous kinematic of displacements, which is shown to be dominated over other preceding theories, is derived from an elasticity formulation, rather by the hypothesis of displacements. The materials are assumed to be graded in two directions and the effective properties are computed using the rule of mixture. Numerical results for deflections and critical buckling load for 2D-FGM plates are presented and analyzed. In general, the results obtained show more complicated than those of one-directional FGM plates, due to the multiple gradation of 2D-FGM. The accuracy of the proposed approach assessed on numerical results has been confirmed by comparisons, which are made against the analytical solutions. A parametric study on the effects of various numerical aspect ratios (e.g., volume fraction, boundary conditions, thickness to length ratio, etc.) on static deflections and critical buckling is presented. Most aspect ratios have strong effects on the mechanical behaviors of 2D FGM plates. The present results may be helpful to the design of 2D FGM in engineering applications. Several potential problems appear worth of further studies, for instance, sandwich plates with 2D-FGM core in thermal environment [41]; and 2D-FGM plates with defects using extended isogeometric analysis [42, 43].

Acknowledgment

The support of Vietnam National Foundation for Science and Technology Development (NAFOSTED) under grant number 107.02-2015.03 is gratefully acknowledged.

References

- [1] P. Liu, T.Q. Bui, D. Zhu, T.T. Yu, J.W. Wang, S.H. Yin, S. Hirose, Buckling failure analysis of cracked functionally graded plates by a stabilized discrete shear gap extended 3-node triangular plate element, *Compos. Part B Eng.* 7 (2015) 179–193.
- [2] N. Valizadeh, S. Natarajan, O.A. Gonzalez-Estrada, T. Rabczuk, Q.T. Bui, P.A.S. Bardas, NURBS-based finite element analysis of functionally graded plates: static bending, vibration, buckling and flutter, *Compos. Struct.* 99 (2013) 309–326.
- [3] J.N. Reddy, Analysis of functionally graded plates, *Int. J. Numer. Methods Eng.* 47 (2000) 663–684.
- [4] A.M. Zenkour, Generalized shear deformation theory for bending analysis of functionally graded plates, *Appl. Math. Model.* 30 (2006) 67–84.
- [5] P. Malekzadeh, S.A. Shojaee, Dynamic response of functionally graded plates under moving heat source, *Compos. Part B* 44 (2013) 295–303.
- [6] P. Malekzadeh, S.M. Monajjemzadeh, Dynamic response of functionally graded plates in thermal environmental under moving load, *Compos. Part B* 45 (2013) 1521–1533.
- [7] T.T. Yu, S.H. Yin, Q.T. Bui, S. Hirose, A simple FSDT-based isogeometric analysis for geometrically nonlinear analysis of functionally graded plates, *Finite Elem. Anal. Des.* 96 (2015) 1–10.
- [8] S.H. Yin, J.S. Hale, T.T. Yu, Q.T. Bui, S.P.A. Bordas, Isogeometric locking-free plate element: a simple first order shear deformation theory for functionally graded plates, *Compos. Struct.* 118 (2015) 121–138.
- [9] S.H. Yin, Y.Y. Yu, Q.T. Bui, N.M. Nguyen, Geometrically nonlinear analysis of functionally graded plates using isogeometric analysis, *Eng. Comput.* 32 (2015) 519–558.
- [10] Q.T. Bui, V.T. Do, T.H.L. Ton, H.D. Doan, S. Tanaka, T.D. Pham, T.A. Nguyen-Van, T.T. Yu, S. Hirose, On the high temperature mechanical behaviors analysis of heated functionally graded plates using FEM and a new third-order shear deformation plate theory, *Compos. Part B Eng.* 92 (2016) 218–241.
- [11] J. Yang, H.S. Shen, Nonlinear bending analysis of shear deformable functionally graded plates subjected to thermo-mechanical loads under various boundary conditions, *Compos. Part B: Eng.* 34 (2003) 103–115.
- [12] M. Nemat-Alla, Reduction of thermal stresses by developing two-dimensional functionally graded materials, *Int. J. Solids Struct.* 40 (2003) 7339–7356.
- [13] J. Aboudi, M. Pindera, S. Arnold, Thermoelasticity theory for bi-directionally functionally graded materials, *J. Therm. Stress* 19 (1996) 809–861.
- [14] J. Aboudi, M. Pindera, S. Arnold, Thermoelastic theory for the response of materials functionally graded in two dimensions, *Int. J. Solids Struct.* 33 (1996) 931–966.
- [15] M. Martin, Numerical solution of the Cauchy problem for steady-state heat transfer in two-dimensional functionally graded materials, *Int. J. Solids Struct.* 42 (2005) 4338–4351.
- [16] M. Nemat-Alla, Reduction of thermal stresses by composition optimization of two-dimensional functionally graded materials, *Acta Mech.* 208 (2009) 147–161.
- [17] M. Nemat-Alla, K.I.E. Ahmed, I. Hassab-Allah, Elastic-plastic analysis of two-dimensional functionally graded materials under thermal loading, *Int. J. Solids Struct.* 46 (2009) 2774–2786.
- [18] M. Asgari, M. Akhlaghi, Natural frequency analysis of 2D-FGM thick hollow cylinder based on three-dimensional elasticity equations, *Eur. J. Mech. A/Solids* 30 (2011) 72–81.
- [19] M.J. Ebrahimi, M.M. Najafzadeh, Free vibration analysis of two-dimensional functionally graded cylindrical shells, *Appl. Math. Model.* 38 (2014) 308–324.
- [20] M. Asgari, M. Akhlaghi, S.M. Hosseini, Dynamic analysis of two-dimensional functionally graded thick hollow cylinder with finite length under impact loading, *Acta Mech.* 208 (2009) 163–180.
- [21] C.F. Lü, C.W. Lim, W.Q. Chen, Semi-analytical analysis for multi-directional functionally graded plates: 3-d elasticity solutions, *Int. J. Numer. Methods Eng.* 79 (2009) 25–44.
- [22] M. Shariyat, R. Jafari, Nonlinear low-velocity impact response analysis of a radially preloaded two-directional functionally graded circular plate: a refined contact stiffness approach, *Compos. Part B: Eng.* 45 (2013) 981–994.
- [23] F.L. Qian, R.C. Batra, Design of bidirectional functionally graded plate for optimal natural frequencies, *J. Sound Vib.* 280 (2005) 415–424.
- [24] S. Satouri, M.H. Kargarnovin, F. Allahkarami, A. Asanjarani, Application of third order shear deformation theory in buckling analysis of 2D-functionally graded cylindrical shell reinforced by axial stiffeners, *Compos. Part B: Eng.* 79 (2015) 236–253.
- [25] R. Pilafkan, D.P. Folkow, M. Darvizeh, A. Darvizeh, Three dimensional frequency analysis of bidirectional functionally graded thick cylindrical shells using a radial point interpolation method (RPIM), *Eur. J. Mech. A/Solids* 39 (2013) 26–34.
- [26] M. Simsek, Bi-directional functionally graded materials (BDFGMs) for free and forced vibration of Timoshenko beams with various boundary conditions, *Compos. Struct.* 133 (2015) 968–978.
- [27] M. Simsek, Buckling of Timoshenko beams composed of two-dimensional functionally graded materials (2D-FGM) having different boundary conditions, *Compos. Struct.* 149 (2016) 304–314.
- [28] D.K. Nguyen, Q.H. Nguyen, T.T. Tran, V.T. Bui, Vibration of bi-dimensional functionally graded Timoshenko beams excited by a moving load, *Acta Mech.* 228 (2017) 141–155.
- [29] M.Z. Nejad, A. Hadi, A. Rastgoo, Buckling analysis of arbitrary two-directional functionally graded Euler-Bernoulli nano-beams based on nonlocal elasticity theory, *Int. J. Eng. Sci.* 103 (2016) 1–10.
- [30] M.Z. Nejad, A. Hadi, Non-local analysis of free vibration of bi-directional functionally graded Euler-Bernoulli nano-beams, *Int. J. Eng. Sci.* 105 (2016) 1–11.
- [31] M. Lezgy-Nazargah, Fully coupled thermo-mechanical analysis of bi-directional

- FGM beams using NURBS isogeometric finite element approach, *Aerosp. Sci. Technol.* 45 (2015) 154–164.
- [32] S.H. Hedia, Comparison of one-dimensional and two-dimensional functionally graded materials for the backing shell of the cemented acetabular cup, *J. Biomed. Mater. Res. Part B: Appl. Biomater.* 74B (2005) 732–739.
- [33] Q.T. Bui, N.M. Nguyen, Ch Zhang, Buckling analysis of Reissner-Mindlin plates subjected to in-plane edge loads using a shear-locking-free and meshfree method, *Eng. Anal. Bound. Elem.* 35 (2011) 1038–1053.
- [34] G. Shi, A new simple third-order shear deformation theory of plates, *Int. J. Solids Struct.* 44 (2007) 4399–4417.
- [35] N. Wattanasakulpong, G.B. Prusty, D.W. Kelly, Free and forced vibration analysis using improved third-order shear deformation theory for functionally graded plates under high temperature loading, *J. Sandw. Struct. Mater.* 15 (2013) 583–606.
- [36] N. Wattanasakulpong, G.B. Prusty, D.W. Kelly, Thermal buckling and elastic vibration of third-order shear deformable functionally graded beams, *Int. J. Mech. Sci.* 53 (2011) 734–743.
- [37] D.H. Doan, T.Q. Bui, D.D. Nguyen, F. Fushinobu, Hybrid phase field simulation of dynamic crack propagation in functionally graded glass-filled epoxy, *Compos. Part B: Eng.* 99 (2016) 266–276.
- [38] D.D. Nguyen, Nonlinear thermal dynamic analysis of eccentrically stiffened S-FGM circular cylindrical shells surrounded on elastic foundations using the Reddy's third-order shear deformation shell theory, *J. Eur. J. Mech. – A/Solids* 58 (2016) 10–30.
- [39] H.C. Pham, D.D. Nguyen, Thermal stability analysis of eccentrically stiffened Sigmoid – FGM plate with metal–ceramic–metal layers based on FSDT, *Cogent Eng.* 3 (1182098) (2016) 1–15.
- [40] D.D. Nguyen, H.B. Dao, H.C. Pham, Nonlinear thermal dynamic response of shear deformable FGM plates on elastic foundations, *J. Therm. Stress* 39 (3) (2016) 278–297.
- [41] V.T. Do, Q.T. Bui, T.T. Yu, T.D. Pham, T.C. Nguyen, Role of material combination and new results of mechanical behavior for FG sandwich plates in thermal environment, *J. Comput. Sci.* 21 (2017) 164–181.
- [42] Q.T. Bui, Extended isogeometric dynamic and static fracture analysis for cracks in piezoelectric materials using NURBS, *Comput. Methods Appl. Mech. Eng.* 295 (2015) 470–509.
- [43] Q.T. Bui, S. Hirose, Ch. Zhang, T. Rabczuk, C.T. Wu, T. Saitoh, J. Lei, Extended isogeometric analysis for dynamic fracture in multiphase piezoelectric/piezomagnetic composites, *Mech. Mater.* 97 (2016) 135–163.